Integrating New GNSS Methods into 3D Ionospheric Imaging: A Simulation Study

SeNSe Lab
Satellite Navigation & Sensing Laboratory
University of Colorado **Boulder**

SWx TREC

COLORADO CENTER FOR ASTRODYNAMICS RESEARCH

Brenna Royersmith, Brian Breitsch, Y. Jade Morton
University of Colorado Boulder

Abstract / Introduction

Background:

- Key issue in previous studies is the limitation of data source(s) with good spatial or temporal resolution, especially difficult to achieve both
- Tomography (3D imaging) allows us to utilize the potential of all sources together to fill data gaps
- Previous research has been done in our lab detecting polar structures using GNSS-R over polar regions and oceans, where receivers are not feasible

Objective:

- Develop a new tomographic algorithm which can ingest reflected satellite signals to improve ionospheric imaging
- Bring together a larger variety of data than previous studies for better quality outputs (including low-elevation)

Method:

- Combine ground-based GNSS and GNSS Radio Occultation (GNSS-RO) with GNSS Reflectometry (GNSS-R), data derived from Precise Orbit Determination (POD), and low-elevation satellite signals
- Using a voxel-based inversion method using IRI2020 (PyIRI) as a base
- New algorithm relies on a forward Voronoi method and simultaneous multiplicative algebraic reconstruction technique (SMART) to produce images

Results:

- Significant improvement of output errors when incorporating low-elevation and reflected signals
- Successful algorithm performance in production of 3D image reconstruction

Background / Objectives

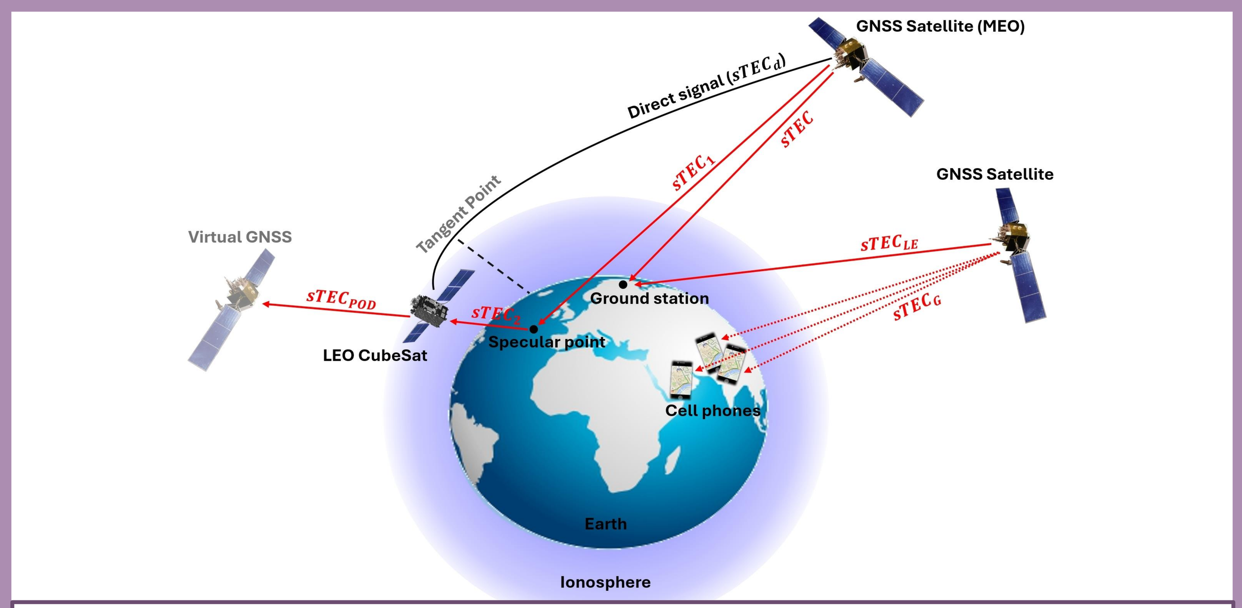

Figure 1. Included data sources in this project: ground-based signals (**sTEC**, **sTEC$_G$**), radio-occulted signals (GNSS-RO) (**sTEC$_G$**), TEC derived from precise orbit determination (**sTEC$_{POD}$**) and newly added reflected (GNSS-R[1]) (**sTEC$_1$** and **sTEC$_2$**) and low elevation signals (**sTEC$_{LE}$**).

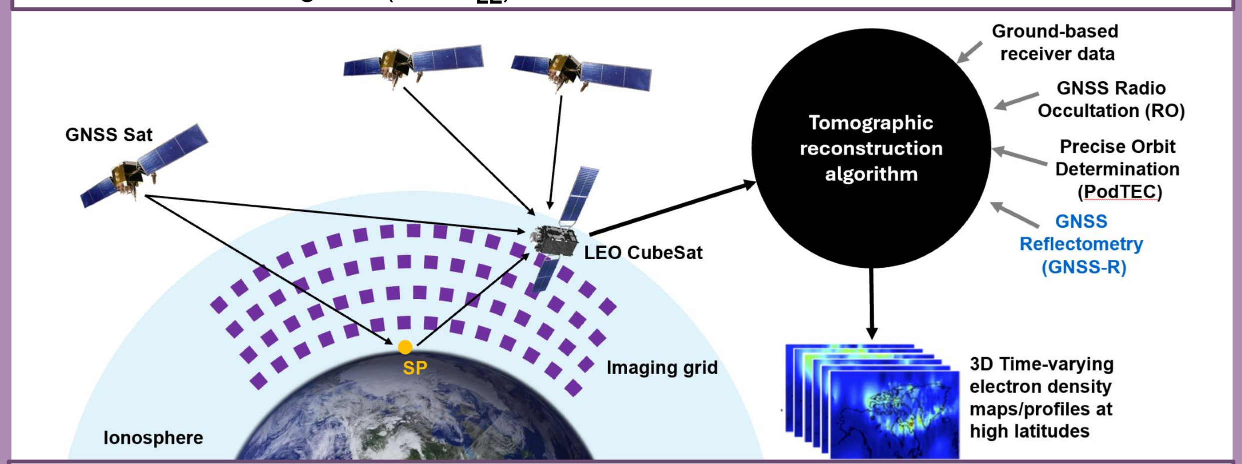

Figure 2. Example of the tomographic process[2]. A model ionosphere is used as a base. Data (simulated here) is collected from rays traveling through the imaging area. These data are assimilated into an algorithm which sorts which measurements intersect the grid (voxels) and where, resulting in an updated model image that better reflects the real data and more accurately represents the ionosphere.

Inversion Method

Voxel-based inversion method:

- Base ionosphere model (IRI2020) is broken into a grid of voxels.
- To keep voxels evenly distributed, stereographic coordinates are used in place of geographic.
- A Voronoi forward method[3] is employed to find the voxel intersections of each ray path.
- Currently searches the entire imaging area for intersections but is being updated to only search neighborhoods around rays to speed up calculation.
- Inversion reconstruction of the image is done using a simultaneous multiplicative algebraic reconstruction technique (SMART)[4].

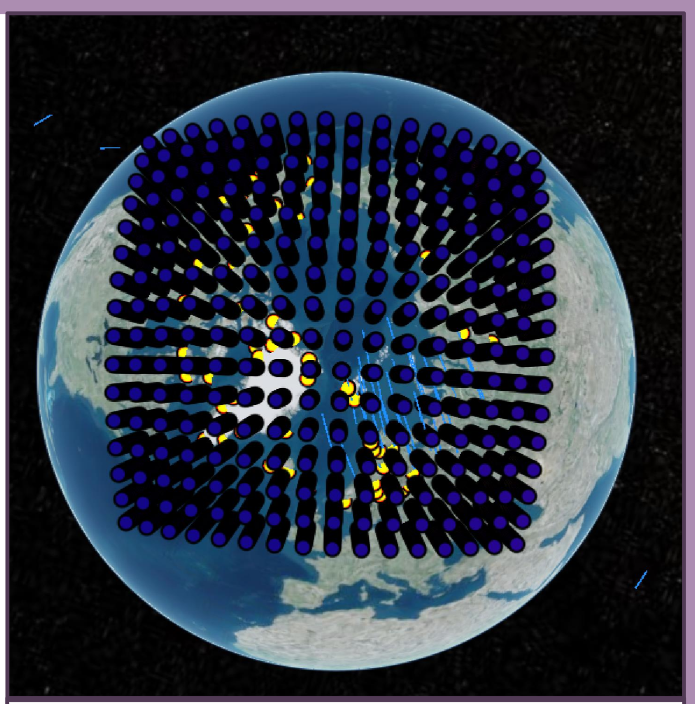

Figure 3. Ionosphere model voxel grid points over the north pole, shown in dark purple. Yellow dots are ground receivers.

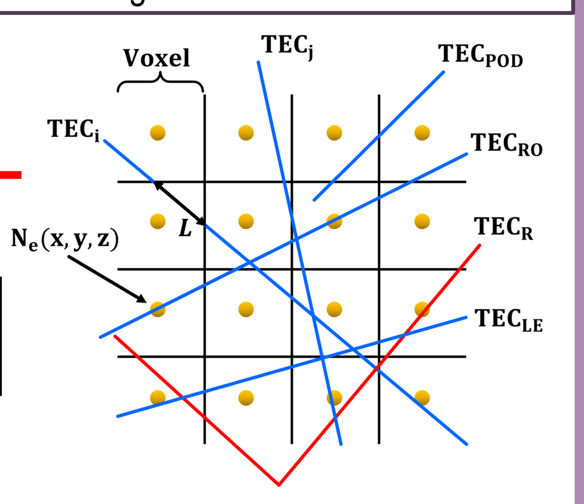

$$\begin{bmatrix} TEC_1 \\ \vdots \\ TEC_N \end{bmatrix} = \begin{bmatrix} L_{1,1} & \cdots & L_{1,NMK} \\ \vdots & \ddots & \vdots \\ L_{N,1} & \cdots & L_{N,NMK} \end{bmatrix} \begin{bmatrix} N_e(x_1,y_1,z_1) \\ \vdots \\ N_e(x_N,y_N,z_N) \end{bmatrix}$$

Inversion: $N_e = H^{-1}TEC$

Figure 4. Visualization of how various ray path geometries (Figure 1) travel through voxels (right) to aid understanding of the main inversion equation (left).

Tomographic Algorithm

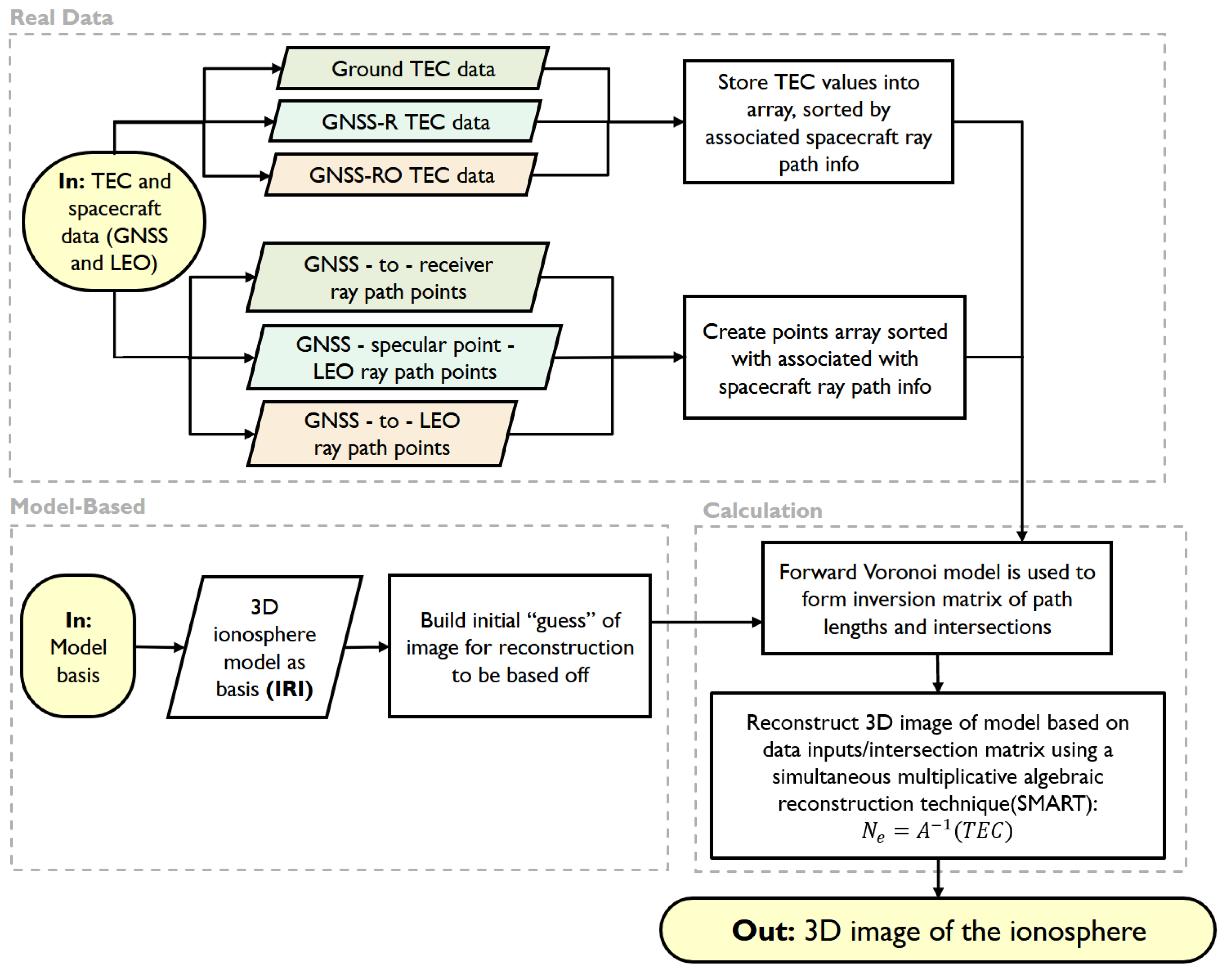

Figure 5. Block diagram explaining the process of our tomographic algorithm, from satellite data/information to resulting image.

Results

Satellite Simulation

- Simulated satellites on real GNSS and Spire CubeSat orbital parameters with real receivers (see **Table 1**)
- Reconstruction is run over a 10-minute period, grid resolution is 500km x 500km x 25km

Error in Reconstruction

- We define "error" as the difference between the base model and the reconstructed image (values in **Table 2**)
- Mean error refers to the average difference. RMSE is the root mean square of the difference.

LEO Constellation	Number of CubeSats	Orbital Planes	Inclination (°)	Altitude (km)
Spire	24	6	97.3	500
GNSS Constellation	**Number of Satellites**	**Orbital Planes**	**Inclination (°)**	**Altitude (km)**
GPS	30	6	55	20,180
GLONASS	24	3	64.8	23,200
GALILEO	24	3	56	19,130

Ground Receivers	Number of Receivers	Category	Latitude Cutoff (°)
IGS	38	High Latitude	55
CHAIN	16	High Latitude	55
Madrigal	29	High Latitude	60
SeNSe	5	High Latitude	55

Table 1. Orbital parameters for GNSS and LEO constellations and ground receiver info.

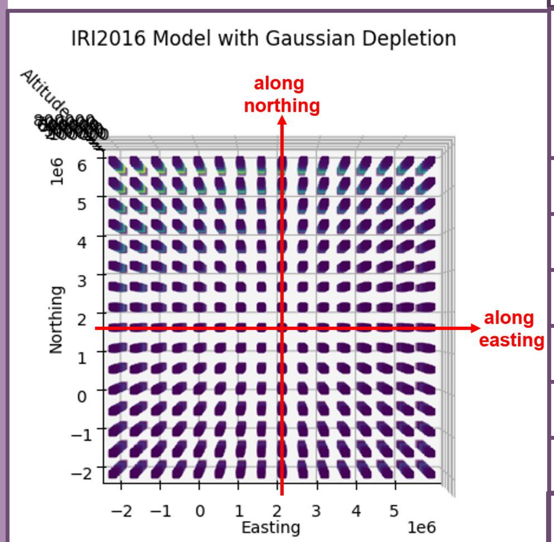

# LEO	Ray #	RMSE w/ GNSS-R ($1e9m^{-3}$)	ME w/ GNSS-R ($1e9m^{-3}$)	RMSEw/o GNSS-R ($1e9m^{-3}$)	ME w/o GNSS-R ($1e9m^{-3}$)	Mean Difference (ref – no ref)
1	6,261	7.55	5.75	8.28	6.14	0.15
5	17,074	7.18	5.11	8.07	5.74	0.42
10	30,809	7.07	4.06	8.05	5.06	0.75
15	44,211	6.58	3.15	7.97	4.51	1.02
20	56,568	6.07	2.81	7.94	4.07	1.19
24	67,228	5.41	2.40	7.84	3.80	1.32

Table 2. Collection of error/RMSE values comparing the addition of ray paths / reflection.

Figure 6 (above). Visual aid for Figure 7: imaging area grid in universal stereographic coordinates. Area sits over the North Pole with longitude 0 at the bottom of the plot. Slices in Figure 7 are taken along the arrows shown and across altitude.

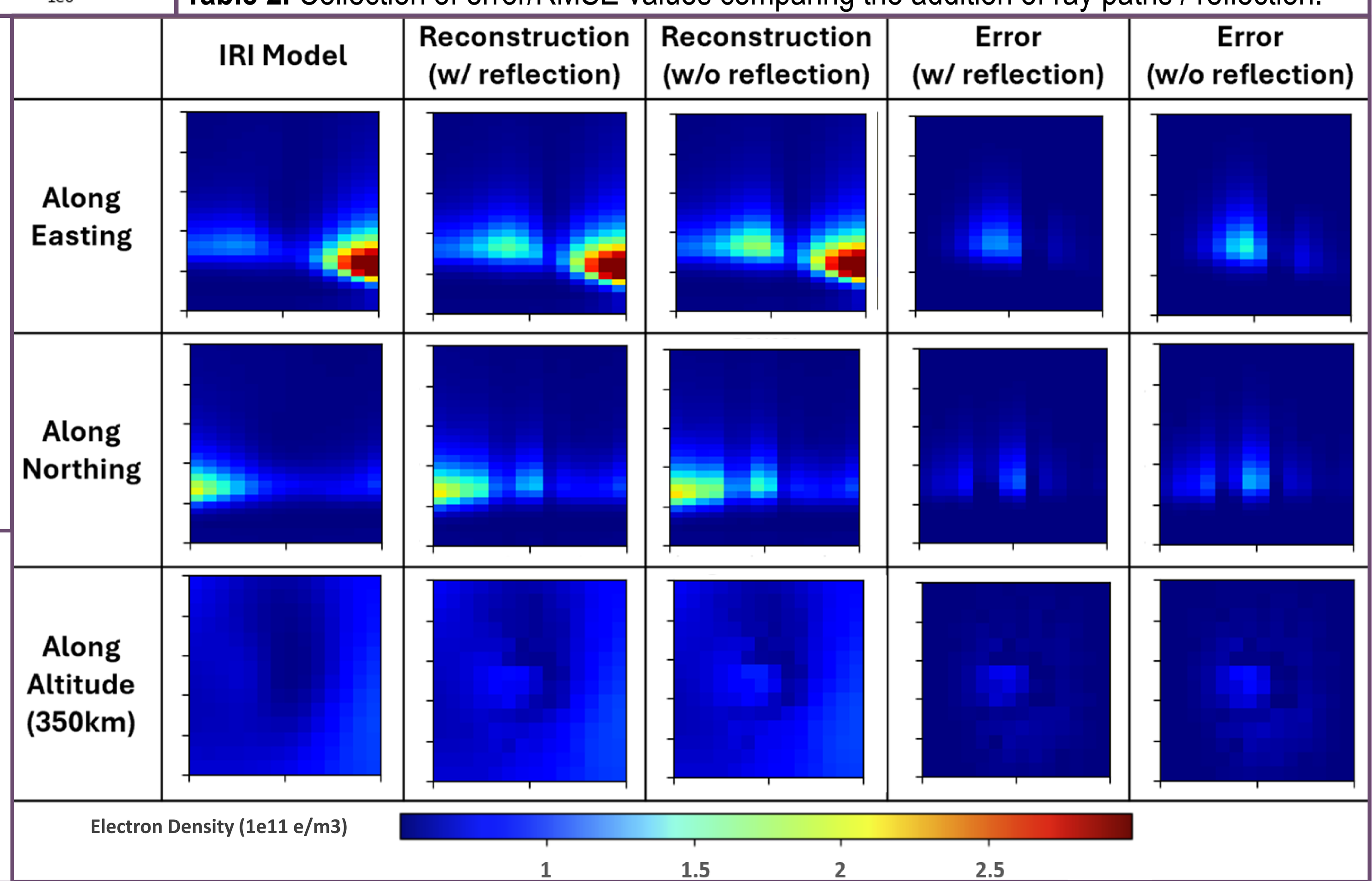

Figure 7 (right). Slices taken from: model, reconstruction (with / without reflection), and error (with / without reflection) along each stereographic direction indicated in Figure 6.

Analysis

Source Type	Total Number of Rays	Low-Elevation Rays	% of low-elev rays out of total	% of total number of rays
Ground	4,397	2,397	54.5 %	6.3 %
GNSS-RO	48,794	35,151	72.0 %	70.4 %
GNSS-R	16,079	7,858	48.9 %	23.3 %
All Rays	69,270	45,406	65.5 %	100 %

Table 3. Total numbers for each data source type, including the number and percentage of low-elevation rays included with each type.

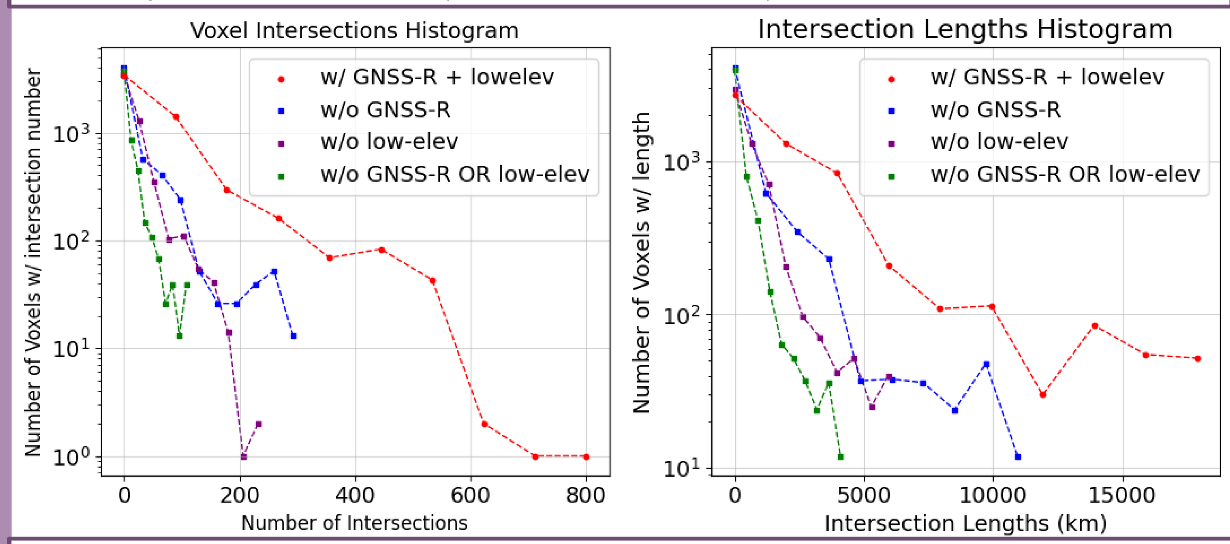

Figure 8. Left: Histogram of voxel intersections, right: Histogram of voxel intersection lengths. Represented for all data conditions indicated by legend.

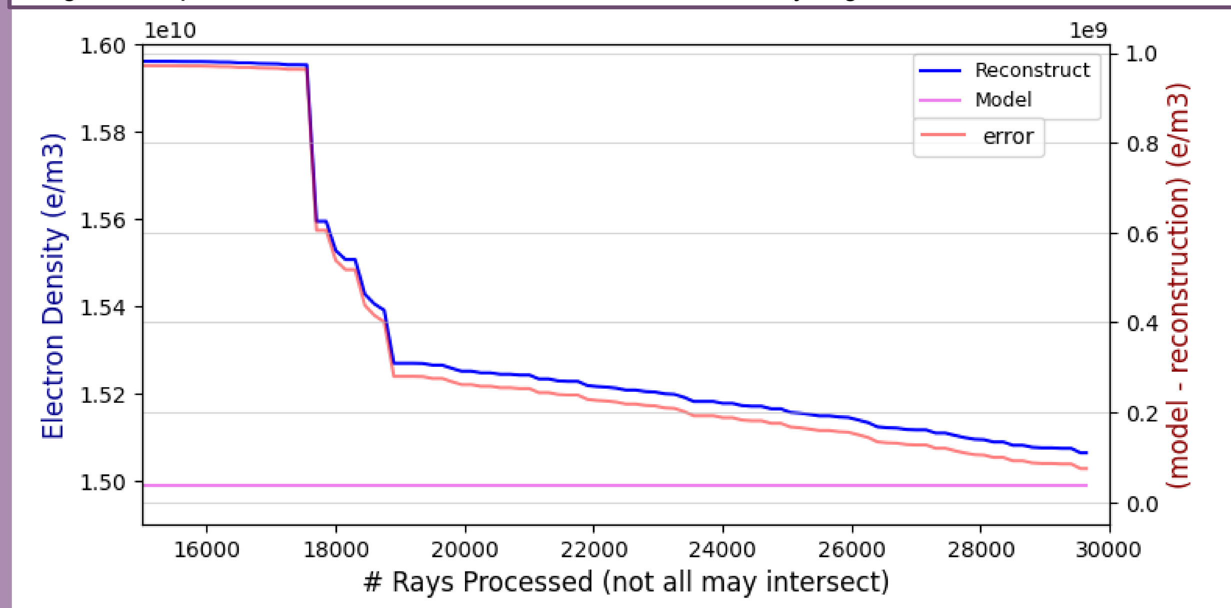

Figure 9. Single-voxel analysis: Voxel with the most intersections was analyzed as ray paths were added 150 at a time to see how reconstruction and error changes.

Conclusions

Results Discussion:

- The new ionospheric tomography algorithm successfully produces 3D images of the ionosphere using simulated satellites and data.
- We see that overall, the more satellites we add, the more the image improves due to more voxel ray path intersections.
- The addition of GNSS-R ray paths alone does improve image quality, but only marginally.
- Low-elevation satellite signals make up over half of the included observables, greatly contributing to the performance of our algorithm

Challenges:

- How to distinguish sTEC along incident and reflected rays when using real data
- Simulation is very optimistic and idealistic, leading to questions about accuracy and feasibility.

Future Work:

- More complete analysis on the impact of low-elevation satellite signals
- Study the possibility of adding covariance matrices to reconstruction for regions with no data intersections
- Real data processing and validation
- Separating incident and reflected sTEC

References and Acknowledgements

[1] C. Zuffada, C. Chew and S. V. Nghiem, "Global Navigation Satellite System Reflectometry (GNSS-R) algorithms for wetland observations," *2017 IEEE International Geoscience and Remote Sensing Symposium (IGARSS)*, Fort Worth, TX, USA, 2017, pp. 1126-1129, doi: 10.1109/IGARSS.2017.8127155.

[2] T. Hu, X. Xu and J. Luo, "A Global CIT Model Fusing Ground-Based GNSS and Space-Borne LEO Satellite Data for Monitoring the Geomagnetic Storm," in *IEEE Transactions on Geoscience and Remote Sensing*, vol. 62, pp. 1-11, 2024, Art no. 5801311, doi: 10.1109/TGRS.2024.3412953.

[3] Franz Aurenhammer. Voronoi diagrams—a survey of a fundamental geometric data structure. ACM Comput. Surv. 23, 3 (1991), 345–405. https://doi.org/10.1145/116873.116880

[4] Gerzen, T. and Minkwitz, D.: Simultaneous multiplicative column-normalized method (SMART) for 3-D ionosphere tomography in comparison to other algebraic methods, Ann. Geophys., 34, 97–115, https://doi.org/10.5194/angeo-34-97-2016, 2016.

This project is funded by ONR contract # N00014-23-1-2145 and others by co-authors. Work is based on previously unpublished algorithms developed by Brian Breitsch, whose help is greatly appreciated and has greatly contributed to this project.

Contact info:
Institution Email : Brenna.Royersmith@colorado.edu